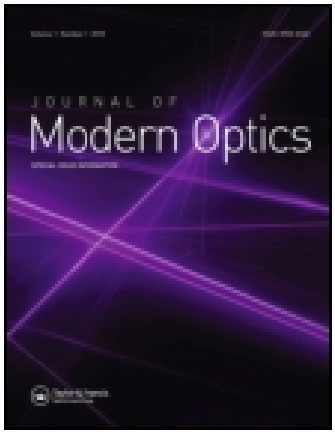

Journal of Modern Optics
Publication details, including instructions for authors and subscription information:
http://www.tandfonline.com/loi/tmop20

An intermediate range solution to a diffraction problem with impedance conditions

Rab Nawaz[a], Abdul Wahab[a] & Amer Rasheed[a]
[a] Department of Mathematics, COMSATS Institute of Information Technology, Wah Cantonment, Pakistan.
Published online: 24 Jun 2014.

Journal of Modern Optics, 2014
Vol. 61, No. 16, 1324–1332, http://dx.doi.org/10.1080/09500340.2014.931477

Taylor & Francis
Taylor & Francis Group

An intermediate range solution to a diffraction problem with impedance conditions

Rab Nawaz*, Abdul Wahab and Amer Rasheed

Department of Mathematics, COMSATS Institute of Information Technology, Wah Cantonment, Pakistan

(*Received 4 April 2014; accepted 23 May 2014*)

An intermediate range solution for the problem of plane wave diffraction by a finite plate with impedance boundaries is presented. Initially, the problem is expressed in terms of two Wiener–Hopf equations with the help of Fourier transform and the boundary conditions in the transformed domain. The consideration of the intermediate range approximation in terms of source position renders integrals that are generally elusive to tackle because of the presence of branch points. These integrals are evaluated by invoking a modified stationary phase method, thereby a field valid over an intermediate range is calculated. The graphical analysis is preformed for various parameters of physical interest for both intermediate and far-field solutions.

Keywords: diffraction; impedance boundary condition; Wiener–Hopf; intermediate range solution

1. Introduction

Acoustic relationships that produce sound and zones of turbulence are exhibited [1] by the diffraction of acoustic quadruples. Curle [2] examined the sound theory by encountering the effects of boundaries in the flow. Since then, many scientists fixated on the surface inhomogeneities with diverse geometries having assorted boundary conditions. In order to cater to various industrial problems, approximate boundary conditions such as absorbing [3] and Myers' impedance conditions [4] attracted shear attention by many researchers and have been used for computational purposes effectively [5–8]. Recently, Ayub et al. [9,10] used first-order impedance conditions to study magnetic line source and point source scattering by impedance and reactive steps. Moreover, a detailed use of higher-order boundary conditions can be found in literature, see for instance [11–13] and articles referred therein. Furthermore, diffraction by a finite strip satisfying Ingard's conditions has been studied by Nawaz [14] whereas diffraction of spherical acoustic wave from an absorbing plane is investigated by Asghar and Hayat [6]. Ayub et al. [7] and Ahmad [8] studied diffraction of sound waves using Myers' boundary conditions and presented improved forms of solutions. Single or multiple diffraction patterns from a strip are presented invoking various analytical, numerical or approximate analytical methods such as geometrical theory of diffraction [15], Kobayashi's potential method [16,17], method of successive approximations [18] and the Wiener–Hopf techniques [19].

In order to put it in a proper context, we highlight the important features of the present investigation. This work is devoted to study a new diffraction problem of a plane acoustic wave incidence on a finite conducting plate. The boundary conditions used in this investigation are of the first-order impedance type which relate wave field and its normal derivative. A detailed exposition of such conditions can be found in the work of Senior and Volkais [20], for example. These conditions are effectively used to model radio wave propagation along the surface of earth and near conducting obstacles. The significance of such conditions is comprehensively established by Pelosi and Ufimtsev [21]. The finite conducting plate occupies the surface $y = 0$, $-l < x < 0$ with a velocity of the moving fluid parallel to the x-axis having magnitude $U > 0$. The fluid is assumed to be flowing uniformly along the plate. The governing equations are linearized and the special effects of viscosity, thermal conductivity and gravity are ignored whereas the fluid is assumed to have a constant density (incompressible fluid) and sound speed c. We precise that the aim is to see the effect of incident wave (which ultimately produces a diffracted field) on the finite conducting plate while considering the impedance boundary conditions. The aforementioned problem is solved rigorously by using the Wiener–Hopf technique. The main feature of the technique

*Corresponding author. Email: rabnawaz@ciitwah.edu.pk

is that it is not fundamentally numerical in nature and thus allows additional insight into the mathematical and physical structure of the diffracted field.

The problem under discussion has wider applications in acoustics and electromagnetics. A strip problem with impedance boundary conditions can also be treated as a mathematical model for a noise barrier lined with different material properties. Such barriers are the better source for the reduction of noise levels at airports or roadsides for instance. The field radiated from the edges of the finite barrier may only affect a receiver in the shadow region of such a barrier which can be done by lining the barrier with different acoustically absorbent materials. The work may also have significant applications in electromagnetism where a thin dielectric layer can be considered on a perfectly conducting finite plate which will act as a waveguide launcher.

The solution to the aforementioned problem is presented in the intermediate range. In far-field approximations, emerging integrals involve the terms of $O(1/\sqrt{kR})$ whereas the consideration of intermediate range approximation in terms of source position retains the terms of $O(1/\sqrt[3]{kR})$ in the expansion of the Hankel function where k is the wavenumber and R is the source to receiver distance. Consideration of such terms leads to more involved integrals in the inverse Fourier transform, which are generally intriguing to handle because of the presence of branch points and are only amenable to solutions using asymptotic approximations (a little discrepancy in the solution is observed for creating values of parameters). The analytic solutions of these integrals are computed by invoking a modified stationary phase technique and the field for an intermediate range in terms of the source position is calculated following the arguments of Noble [22]. In this investigation, the integral transforms, Wiener–Hopf technique [19] and asymptotic methods [23] are blended to compute the diffracted field. The far-field results can be regarded as a limiting case when the source position is shifted from intermediate range to a far off range, that is, when the terms of $O(1/\sqrt[3]{kR})$ are neglected. A graphical comparison between the far field and the intermediate field is presented for different physical parameters. Certainly, the intermediate range solution provides further insight of the diffracted field as compared to the far-field solution.

The rest of the paper is organized in following manner. In Section 2, the diffraction problem is mathematically formulated. The standard Wiener–Hopf functional equations are constructed in the transformed domain in Section 3. Section 4 is dedicated to the Wiener–Hopf procedure to resolve the transformed functional equations. Section 5 deals with an intermediate approximation of the diffracted field. A few numerical illustrations are provided in Section 6. The paper ends with a few concluding remarks in Section 7.

2. Mathematical formulation

The model problem consists of a plane wave incidence on an impedance finite conducting plate ($-l \le x \le 0$, $y = 0$ where l is the strip length) which is encountering a small gust with uniform flow parallel to it with velocity amplitude U. The plate is supposed to be infinitely thin and straight. We decompose the total field Ψ_e^t as

$$\Psi_e^t(x, y) = \Psi_i(x, y) + \Psi_r(x, y) + \Psi_e(x, y), \quad (1)$$

where Ψ_i and Ψ_r are the plane wave incident and reflected fields, respectively, at $y = 0$ and are given by

$$\Psi_i(x, y) = \exp\left[-ik(x\cos\theta_0 + y\sin\theta_0)\right], \quad (2)$$

and

$$\Psi_r(x, y) = \left(\frac{1 - \beta_1\sin\theta_0}{1 + \beta_1\sin\theta_0}\right)\exp[-ik(x\cos\theta_0 - y\sin\theta_0)], \quad (3)$$

for all $(x, y) \in \mathbb{R}^2$, where β_1 is the admittance parameter and θ_0 is the incidence angle. The diffracted field Ψ_e is the solution to the Helmholtz equation

$$\left(\frac{\partial^2}{\partial x^2} + \frac{\partial^2}{\partial y^2} + k^2\right)\Psi_e(x, y) = 0, \qquad (x, y) \in \mathbb{R}^2. \quad (4)$$

Here k is the free-space wavenumber such that $k = k_1 + ik_2$ with $(0 < k_2 \ll k_1)$ and the time dependence is $e^{-i\omega t}$. The medium is assumed to be slightly lossy and the solution for real k is achieved by letting $k_2 \to 0$.

The boundary conditions on a transmissive finite plate are the first-order impedance (Leontovich) conditions relating field and its normal derivative and sometimes also stated as standard impedance boundary conditions [12]. Mathematically, the first-order impedance conditions are given by

$$\left(\frac{\partial}{\partial n} - ik\frac{z}{\beta_1}\right)\phi = 0, \quad (5)$$

where ϕ is the velocity potential, β_1 is the normal specific impedance of the material relative to the impedance of the surrounding medium such that $\Re e\{\beta_1\} > 0$ whereas z is the intrinsic impedance of the surrounding medium. Here, $\partial/\partial n$ represents the normal derivative where n is outward unit normal to the boundary.

As we are interested in finding the diffracted field due to plane wave incidence on the impedance finite plate, mixed type Neumann and Dirichlet conditions are taken along the plate line. Therefore, the total diffracted field Ψ_e^t can be determined with the following boundary and continuity conditions

$$\left(1 \pm \frac{\beta_1}{ik}\frac{\partial}{\partial y}\right)\Psi_e^t(x, 0^{\pm}) = 0, \quad x \in [-l, 0], \quad (6)$$

$$\Psi_e^t(x, 0^+) = \Psi_e^t(x, 0^-), \quad x \in \mathbb{R} \setminus [-l, 0], \quad (7)$$

$$\frac{\partial}{\partial y}\Psi_e^t(x, 0^+) = \frac{\partial}{\partial y}\Psi_e^t(x, 0^-), \quad x \in \mathbb{R} \setminus [-l, 0]. \quad (8)$$

The above equations are the admissible conditions from the mathematical point of view and are acoustic counterpart of those satisfied by an electrically resistive finite plate. The modeling of propagation of radio waves along the surface of earth and near conducting barriers is an area where these impedance boundary conditions can be used. Further importance and applications are discussed and explained in [24]. Moreover, the time harmonic factor $e^{-i\omega t}$ is suppressed throughout the analysis.

3. Construction of Wiener–Hopf functional equations

The Wiener–Hopf technique has been the object of the scientific attention of many researchers and due to this technique, many important developments have been achieved. Likewise, in Equations (18)–(19), a vast variety of physically relevant problems can be expressed in terms of the equation originally solved by Wiener and Hopf or to strictly connected ones. In diffraction problems, a fundamental approach due to Jones [25] applies the Laplace transforms directly to the partial differential equations, and the complex variable functional equations are so obtained without having to formulate an integral equation before. The approach taken by Jones [25] has been adopted systematically in many diffraction problems, see for instance [7,8,14,22,26]. Therefore, in order to obtain the solution using a Wiener–Hopf technique, we adopt the Jones approach by which we first transform the boundary value problem (4)–(8) in this section using Fourier transform with respect to variable x thereby constructing the associated Wiener–Hopf functional equations. Precisely, let us introduce

$$\begin{aligned}\overline{\Psi}_e(\alpha, y) &= \frac{1}{\sqrt{2\pi}}\int_{-\infty}^{\infty}\Psi_e(x, y)e^{i\alpha x}dx \\ &= \overline{\Psi}_{e+}(\alpha, y) + e^{-i\alpha l}\overline{\Psi}_{e-}(\alpha, y) + \overline{\Psi}_{e1}(\alpha, y),\end{aligned} \tag{9}$$

where $\alpha = \Re e\{\alpha\} + i\Im m\{\alpha\} = \sigma + i\tau$ and

$$\begin{cases}\overline{\Psi}_{e+}(\alpha, y) = \dfrac{1}{\sqrt{2\pi}}\displaystyle\int_{0}^{\infty}\Psi_e(x, y)e^{i\alpha x}dx, \\ \overline{\Psi}_{e-}(\alpha, y) = \dfrac{1}{\sqrt{2\pi}}\displaystyle\int_{-\infty}^{-l}\Psi_e(x, y)e^{i\alpha(x+l)}dx, \\ \overline{\Psi}_{e1}(\alpha, y) = \dfrac{1}{\sqrt{2\pi}}\displaystyle\int_{-l}^{0}\Psi_e(x, y)e^{i\alpha x}dx.\end{cases}$$

Note that the asymptotic behavior of $\Psi_e(x, y)$ as $|x| \to \infty$ is

$$\Psi_e(x, y) = \begin{cases} O\left(\exp(-ikx)\right), \\ O\left(\exp(-kx\cos\theta_0)\right)\end{cases} \tag{10}$$

whereas $\overline{\Psi}_{e-}(\alpha, y)$ is an analytic and non-zero function of α in the region $\Im m\{\alpha\} < \Im m\{k\}$, $\overline{\Psi}_{e+}(\alpha, y)$ is regular in $\Im m\{\alpha\} > -\Im m\{k\}$ and $\overline{\Psi}_{e1}(\alpha, y)$ is analytic in the common region $-\Im m\{k\} < \Im m\{\alpha\} < \Im m\{k\}$ providing the analytic region in the given strip, for the use of Wiener–Hopf technique.

For a plane wave incident on a finite plate, the incident field (2) is given in the transformed domain as

$$\overline{\Psi}_i(\alpha, 0) = \frac{\exp\left[ikl(\cos\theta_0 - \alpha)\right] - 1}{ik(\cos\theta_0 - \alpha)}. \tag{11}$$

Similarly, the reflected field Ψ_r at $y = 0$ in the transformed domain α is given by

$$\overline{\Psi}_r(\alpha, 0) = \left(\frac{1 - \beta_1\sin\theta_0}{1 + \beta_1\sin\theta_0}\right)\frac{i\left[\exp[ikl(\cos\theta_0 - \alpha)] - 1\right]}{k(\cos\theta_0 - \alpha)}. \tag{12}$$

The Helmholtz Equation (4) is given in the transformed domain by

$$\left(\frac{d^2}{dy^2} + \gamma^2\right)\overline{\Psi}(\alpha, y) = 0, \tag{13}$$

where $\gamma(\alpha) = \sqrt{k^2 - \alpha^2}$ with $\Re e\{\gamma(\alpha)\} > 0$. Equation (13) is the wave equation in the transformed domain which is valid for any α in the strip $-k_2 < \Im\{\alpha\} < k_2\cos\theta_0$. The Fourier transform of boundary conditions (6)–(8) yields

$$\begin{aligned}\overline{\Psi}'_{e1}(\alpha, 0^+) = &-\frac{ik}{\beta_1}\left[\overline{\Psi}_i(\alpha, 0) + \overline{\Psi}_r(\alpha, 0)\right] \\ &- \left[\overline{\Psi}'_i(\alpha, 0) + \overline{\Psi}'_r(\alpha, 0)\right] - \frac{ik}{\beta_1}\overline{\Psi}_{e1}(\alpha, 0^+),\end{aligned} \tag{14}$$

$$\begin{aligned}\overline{\Psi}'_{e1}(\alpha, 0^-) = &\frac{ik}{\beta_1}\left[\overline{\Psi}_i(\alpha, 0) + \overline{\Psi}_r(\alpha, 0)\right] \\ &- \left[\overline{\Psi}'_i(\alpha, 0) + \overline{\Psi}'_r(\alpha, 0)\right] + \frac{ik}{\beta_1}\overline{\Psi}_{e1}(\alpha, 0^-),\end{aligned} \tag{15}$$

and

$$\begin{cases}\overline{\Psi}_{e-}(\alpha, 0^+) = \overline{\Psi}_{e-}(\alpha, 0^-) = \overline{\Psi}_{-}(\alpha, 0), \\ \overline{\Psi}_{e+}(\alpha, 0^+) = \overline{\Psi}_{e+}(\alpha, 0^-) = \overline{\Psi}_{+}(\alpha, 0), \\ \overline{\Psi}'_{e-}(\alpha, 0^+) = \overline{\Psi}'_{e-}(\alpha, 0^-) = \overline{\Psi}'_{e-}(\alpha, 0), \\ \overline{\Psi}'_{e+}(\alpha, 0^+) = \overline{\Psi}'_{e+}(\alpha, 0^-) = \overline{\Psi}'_{e+}(\alpha, 0).\end{cases} \tag{16}$$

Note that the solution of Equation (13) satisfying radiation condition as $|x| \to \infty$ is given by

$$\overline{\Psi}_e(\alpha, y) = \begin{cases} A_1(\alpha)e^{i\gamma y}, & y \geq 0, \\ A_2(\alpha)e^{-i\gamma y}, & y < 0.\end{cases} \tag{17}$$

Omitting the detailed calculations for brevity, by virtue of Equations (14)–(17), we arrive at

$$\begin{aligned}&\overline{\Psi}'_{e+}(\alpha, 0) + e^{-i\alpha l}\overline{\Psi}'_{e-}(\alpha, 0) - i\gamma(\alpha)L(\alpha)J_1(\alpha, 0) \\ &\quad = \overline{\Psi}'_i(\alpha, 0) + \overline{\Psi}'_r(\alpha, 0),\end{aligned} \tag{18}$$

$$\begin{aligned}&\overline{\Psi}_{e+}(\alpha, 0) + e^{-i\alpha l}\overline{\Psi}_{e-}(\alpha, 0) + \frac{\beta_1}{ik}L(\alpha)J'_1(\alpha, 0) \\ &\quad = \overline{\Psi}_i(\alpha, 0) + \overline{\Psi}_r(\alpha, 0),\end{aligned} \tag{19}$$

where

$$J_1(\alpha,0)=\frac{1}{2}\left[\overline{\Psi}_{e1}(\alpha,0^+)-\overline{\Psi}_{e1}(\alpha,0^-)\right], \quad (20)$$

$$J_1'(\alpha,0)=\frac{1}{2}\left[\overline{\Psi}'_{e1}(\alpha,0^+)-\overline{\Psi}'_{e1}(\alpha,0^-)\right], \quad (21)$$

$$L(\alpha)=\left(1+\frac{k}{\beta_1\gamma(\alpha)}\right), \quad (22)$$

and

$$A_1(\alpha)=J_1(\alpha,0)+\frac{J_1'(\alpha,0)}{i\gamma}, \quad (23)$$

$$A_2(\alpha)=-J_1(\alpha,0)+\frac{J_1'(\alpha,0)}{i\gamma}. \quad (24)$$

Equations (18)–(19) are the standard Wiener–Hopf functional equations. In next section, we adopt the Wiener–Hopf procedure to resolve (18)–(19).

4. Wiener–Hopf solution

Equations (18)–(19) represent the three-part boundary value problem and one cannot solve these equations by using any conventional method such as standard integral transform or separation of variable. Here, a standard Wiener–Hopf procedure is adopted by using the factorization

$$L(\alpha)=\left(1+\frac{k}{\beta_1\gamma(\alpha)}\right)=L_+(\alpha)L_-(\alpha), \quad (25)$$

and

$$\gamma(\alpha)=\gamma_+(\alpha)\gamma_-(\alpha), \quad (26)$$

where $L_+(\alpha)$ and $\gamma_+(\alpha)$ are analytic and non-zero in the domain $\Im m\{\alpha\} > -\Im m\{k\}$, that is, for upper half plane while $L_-(\alpha)$ and $\gamma_-(\alpha)$ are analytic and non-zero in the region $\Im m\{\alpha\} < \Im m\{k\}$, that is, lower half plane. The above factorization is achieved by following the factorization procedure as discussed by Asghar et al. [24].

By using the value of $J_1(\alpha,0)$ and $J_1'(\alpha,0)$ from Equations (18)–(19), into (23) and (24), it is found that

$$\begin{aligned}A_1(\alpha)=&\frac{1}{i\gamma\ L(\alpha)}(\overline{\Psi}'_{e+}(\alpha,0)+e^{-i\alpha l}\overline{\Psi}'_{e-}(\alpha,0)\\&-\overline{\Psi}'_i(\alpha,0)-\overline{\Psi}'_r(\alpha,0))\\&-\frac{ik}{\beta_1 L(\alpha)}(\overline{\Psi}_+(\alpha,0)+e^{-i\alpha l}\overline{\Psi}_-(\alpha,0)\\&-\overline{\Psi}_i(\alpha,0)-\overline{\Psi}_r(\alpha,0)),\end{aligned} \quad (27)$$

and

$$\begin{aligned}A_2(\alpha)=&-\frac{1}{i\gamma L(\alpha)}(\overline{\Psi}'_{e+}(\alpha,0)+e^{-i\alpha l}\overline{\Psi}'_{e-}(\alpha,0)\\&-\overline{\Psi}'_i(\alpha,0)-\overline{\Psi}'_r(\alpha,0))\\&-\frac{ik}{\beta_1 L(\alpha)}(\overline{\Psi}_+(\alpha,0)+e^{-i\alpha l}\overline{\Psi}_-(\alpha,0)\\&-\overline{\Psi}_i(\alpha,0)-\overline{\Psi}_r(\alpha,0)).\end{aligned} \quad (28)$$

Making use of Equations (11) and (12) in Equations (18) and (19), we obtain

$$\begin{aligned}&\overline{\Psi}'_{e+}(\alpha,0)+e^{-i\alpha l}\overline{\Psi}'_{e-}(\alpha,0)+S(\alpha)J_1(\alpha,0)\\&\quad=\frac{hb[\exp[ikl(\cos\theta_0-\alpha)]-1]}{(\cos\theta_0-\alpha)},\end{aligned} \quad (29)$$

and

$$\begin{aligned}&\overline{\Psi}_{e+}(\alpha,0)+e^{-i\alpha l}\overline{\Psi}_{e-}(\alpha,0)+\frac{\beta_1}{ik}L_+(\alpha)L_-(\alpha)J_1'(\alpha,0)\\&\quad=-\frac{b[\exp[ikl(\cos\theta_0-\alpha)]-1]}{ik(\cos\theta_0-\alpha)},\end{aligned} \quad (30)$$

where

$$b=\left[\left(\frac{1-\beta_1\sin\theta_0}{1+\beta_1\sin\theta_0}\right)-1\right] \quad \text{and} \quad h=\sin\theta_0.$$

Here

$$S(\alpha)=-i\gamma(\alpha)L(\alpha)=S_+(\alpha)S_-(\alpha), \quad (31)$$

where $S_+(\alpha)=(k+\alpha)^{1/2}L_+(\alpha)$ and $S_-(\alpha)=(k-\alpha)^{1/2}L_-(\alpha)$ are regular in upper and lower half planes ($\alpha=\sigma+i\tau,\ -k_2<\tau<-k_2\cos\theta_0$), respectively.

Equations (29) and (30) are similar to the one already discussed in the monograph by Noble [22] and investigations based on his approach are utilized to get an approximate solution in the intermediate range. The terms of Equations (29)–(30) with negative sign on one side of the equation are equated with the terms with positive sign on the other side, which in result will be equal to a same entire function say $J(\alpha)$. By the analytic continuation and extended form of Liouville's theorem, $J(\alpha)$ can be extended throughout the complex α-plane and the polynomial that is represented by the entire function $J(\alpha)$ is equated to zero. Ignoring the details for brevity and following the procedure given in [22], finally it is found that

$$\overline{\Psi}'_{e+}(\alpha,0)=\frac{bhS_+(\alpha)}{\sqrt{2\pi}}\left[G_1(\alpha)+T(\alpha)C_1\right], \quad (32)$$

$$\overline{\Psi}'_{e-}(\alpha,0)=\frac{bhS_-(\alpha)}{\sqrt{2\pi}}\left[G_2(-\alpha)+T(-\alpha)C_2\right], \quad (33)$$

$$\overline{\Psi}_{e+}(\alpha,0)=-\frac{b\beta_1L_+(\alpha)}{\sqrt{2\pi}k}\left[G_1'(\alpha)+T(\alpha)C_1'\right], \quad (34)$$

$$\overline{\Psi}_{e-}(\alpha,0)=\frac{b\beta_1L_-(\alpha)}{\sqrt{2\pi}k}\left[G_2'(-\alpha)-T(-\alpha)C_2'\right], \quad (35)$$

where

$$\begin{aligned}G_1(\alpha)=&\frac{1}{(\alpha-\cos\theta_0)}\\&\times\left[\frac{1}{S_+(\cos\theta_0)}-\frac{1}{S_+(\alpha)}\right]-e^{-il\cos\theta_0}R_1(\alpha),\end{aligned} \quad (36)$$

$$\begin{aligned}G_2(\alpha)=&\frac{e^{-il\cos\theta_0}}{(\alpha-\cos\theta_0)}\left[\frac{1}{S_+(-\cos\theta_0)}-\frac{1}{S_+(\alpha)}\right]\\&-R_2(\alpha),\end{aligned} \quad (37)$$

$$C_1 = S_+(k)\left[\frac{G_2(k) + S_+(k)G_1(k)\,T(k)}{1 - S_+^2(k)T^2(k)}\right], \quad (38)$$

$$C_2 = S_+(k)\left[\frac{G_1(k) + S_+(k)G_2(k)\,T(k)}{1 - S_+^2(k)T^2(k)}\right], \quad (39)$$

and

$$G_1'(\alpha) = \frac{ik}{(\alpha + \cos\theta_0)}\left[\frac{1}{L_+(-\cos\theta_0)} - \frac{1}{L_+(\alpha)}\right] - e^{-il\cos\theta_0}R_1(\alpha), \quad (40)$$

$$G_2'(\alpha) = \frac{e^{-il\cos\theta_0}}{(\alpha - \cos\theta_0)}\left[\frac{\alpha}{L_+(\alpha)} + \frac{\cos\theta_0}{L_+(\cos\theta_0)}\right] - R_2(\alpha), \quad (41)$$

$$C_1' = L_+(k)\left[\frac{G_2'(k) + L_+(k)G_1'(k)\,T(k)}{1 - L_+^2(k)T^2(k)}\right], \quad (42)$$

$$C_2' = L_+(k)\left[\frac{G_1'(k) + L_+(k)G_2'(k)\,T(k)}{1 - L_+^2(k)T^2(k)}\right]. \quad (43)$$

Here

$$\begin{cases} R_1(\alpha) \\ = \dfrac{E_{-1}[W_{-1}\{-i\,(k+\cos\theta_0)\,l\} - W_{-1}\{-i\,(k+\alpha)\,l\}]}{2\pi i(\alpha - \cos\theta_0)}, \\ R_{1,2}(\alpha) \\ = \dfrac{E_{-1}[W_{-1}\{-i\,(k-\cos\theta_0)\,l\} - W_{-1}\{-i\,(k+\alpha)\,l\}]}{2\pi i(\alpha + \cos\theta_0)}, \end{cases} \quad (44)$$

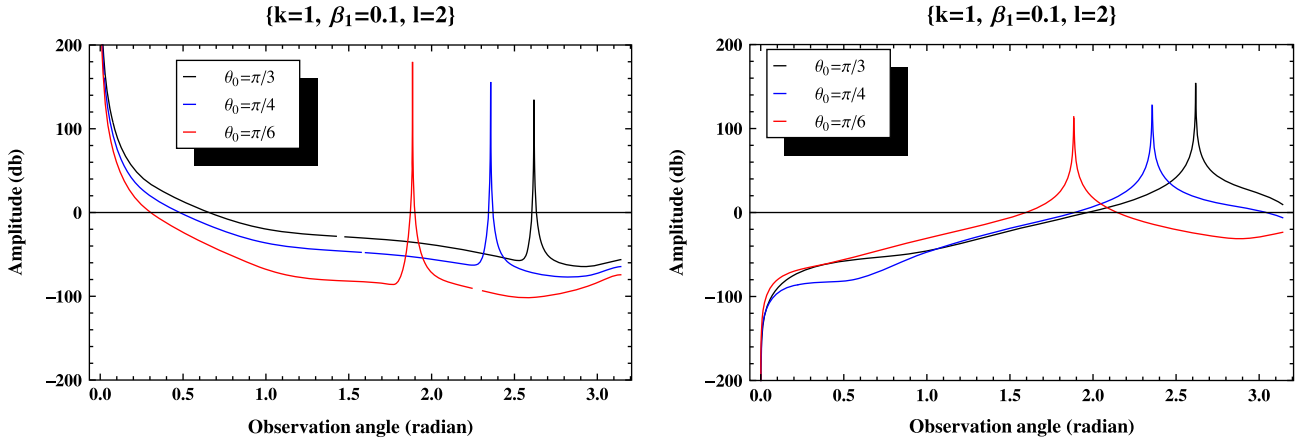

(*a*) Intermediate range solution (*b*) Far-field solution

Figure 1. Amplitude of the diffracted field vs. the observation angle for different values of the incidence angle θ_0 when $k = 1, l = 2$ and $\beta_1 = 0.1$. (The colour version of this figure is included in the online version of the journal.)

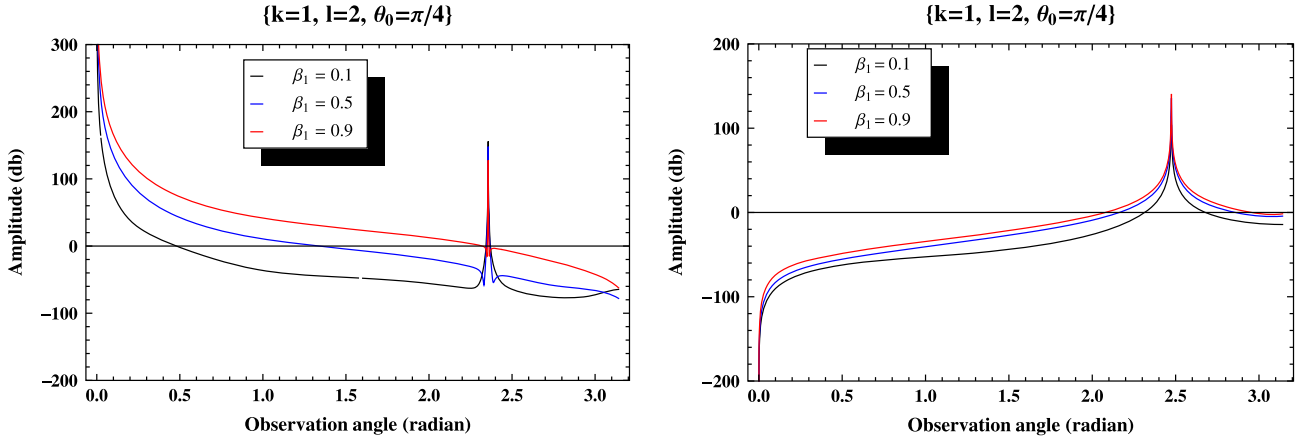

(*a*) Intermediate range solution (*b*) Far-field solution

Figure 2. Amplitude of the diffracted field vs. the observation angle for different values of admittance parameter β_1 when $k = 1, l = 2$ and $\theta_0 = \frac{\pi}{4}$. (The colour version of this figure is included in the online version of the journal.)

$$T(\alpha) = \frac{1}{2\pi i} E_{-1} W_{-1}\{-i(k+\alpha)l\}, \tag{45}$$

$$E_{-1} = 2e^{i\frac{\pi}{4}} e^{ikl} i^{-1} l^{1/2} h_{-1}, \tag{46}$$

$$W_{n-\frac{1}{2}}(p) = \int_0^\infty \frac{u^n e^{-u}}{u+p} du = \Gamma(n+1)\, e^{z/2} z^{n/2-1/2} W_{-\frac{1}{2}(n+1),\frac{1}{2}n}(p), \tag{47}$$

with $p = -i(k+\alpha)l$, $n = -1/2$ and $W_{m,n}$ is known as a *Whittaker function*.

Now making use of Equations (32)–(35) in Equations (27)–(28), it is found that

$$\begin{cases} A_1(\alpha) = \dfrac{1}{\sqrt{2\pi} i\gamma(\alpha) L(\alpha)} \left\{ \begin{array}{l} S_+(\alpha)G_1(\alpha) + S_+(\alpha)T(\alpha)C_1 + e^{-i\alpha l} S_-(\alpha) \\ \times [G_2(-\alpha) + T(-\alpha)C_2] - \frac{hb(1-e^{-il(\cos\theta_0-\alpha)})}{(\cos\theta_0-\alpha)} \end{array} \right\} \\ -\dfrac{ik}{\sqrt{2\pi}\beta_1 L(\alpha)} \left\{ \begin{array}{l} L_+(\alpha)G_1'(\alpha) + T(\alpha)L_+(v)C_1' + e^{-i\alpha l} \\ \times\Big[\big(L_-(\alpha)G_2'(-\alpha) + T(-\alpha)L_+(v)C_2'\big)\Big] - \frac{b\left(1-e^{-il(\cos\theta_0-\alpha)}\right)}{k(\cos\theta_0-\alpha)} \end{array} \right\}, \\ A_2(\alpha) = \dfrac{-1}{\sqrt{2\pi} i\gamma(\alpha) L(\alpha)} \left\{ \begin{array}{l} S_+(\alpha)G_1(\alpha) + S_+(\alpha)T(\alpha)C_1 + e^{-i\alpha l} S_-(\alpha) \\ \times [G_2(-\alpha) + T(-\alpha)C_2] - \frac{hb(1-e^{-il(\cos\theta_0-\alpha)})}{(\cos\theta_0-\alpha)} \end{array} \right\} \\ -\dfrac{ik}{\sqrt{2\pi}\beta_1 L(\alpha)} \left\{ \begin{array}{l} L_+(\alpha)G_1'(\alpha) + T(\alpha)L_+(v)C_1' + e^{-i\alpha l} \\ \times\Big[\big(L_-(\alpha)G_2'(-\alpha) + T(-\alpha)L_+(v)C_2'\big)\Big] - \frac{b\left(1-e^{-il(\cos\theta_0-\alpha)}\right)}{k(\cos\theta_0-\alpha)} \end{array} \right\}, \end{cases} \tag{48}$$

The expression includes the effect of impedance parameter β, where $\beta = 1/\beta_1$, that can also be seen from the solution. Now, we shall derive a diffracted field expression explicitly in the real space by using the results obtained in (48). The diffracted acoustic field $\Psi_e(x, y)$ is obtained by taking the inverse Fourier transform of Equation (17), that is,

$$\Psi_e(x, y) = \frac{1}{\sqrt{2\pi}} \int_{-\infty}^{\infty} \left\{ \begin{array}{l} A_1(\alpha) \\ A_2(\alpha) \end{array} \right\} \exp(i\gamma|y| - i\alpha x) d\alpha, \tag{49}$$

where $A_1(\alpha)$ and $A_2(\alpha)$ are given in Equation (48).

5. Intermediate range approximations

The diffracted field in the intermediate range may now be calculated by evaluating the integrals appearing in Equation (49), asymptotically [23]. Let us introduce the polar coordinates as $x = R\cos\theta$, $|y| = R\sin\theta$ and deform the contour by the transformation $\alpha = -k\cos(\theta + iq)$, $(0 < \theta < \pi, -\infty < q < \infty)$. Then, the Equation (49) reduces to

$$\Psi_e(x, y) = \frac{1}{\sqrt{2\pi}} \int_{-\infty}^{\infty} \left\{ \begin{array}{l} A_1(-k\cos(\theta + iq)) \\ A_2(-k\cos(\theta + iq)) \end{array} \right\} e^{ikR\cosh q} dq. \tag{50}$$

In order to get intermediate range solution, the Maclaurin's series expansions of the terms $A_1(-k\cos(\theta + iq))$and

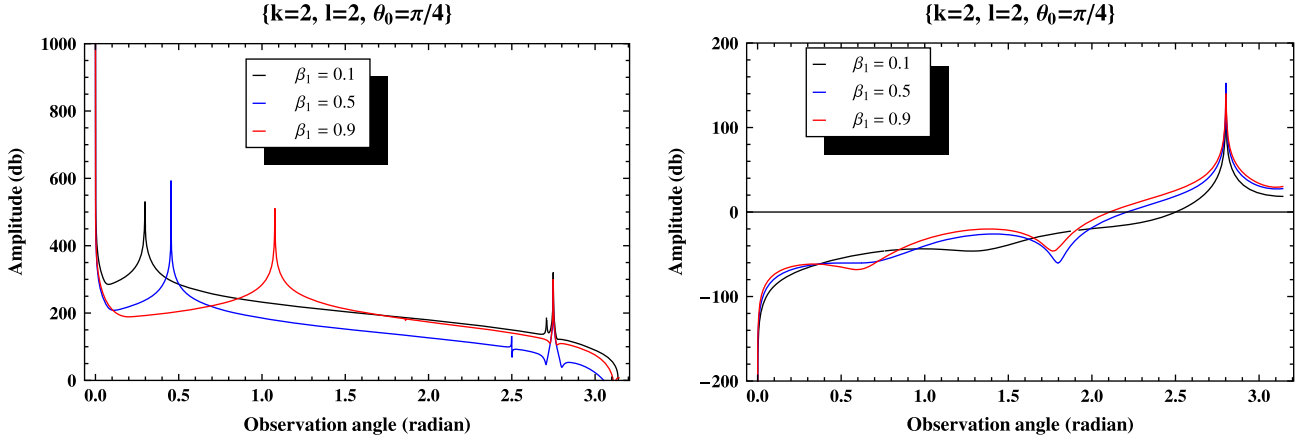

(*a*) Intermediate range solution (*b*) Far-field solution

Figure 3. Amplitude of the diffracted field vs. the observation angle for different values of admittance parameter β_1 when $k = 2$, $l = 2$ and $\theta_0 = \frac{\pi}{4}$. (The colour version of this figure is included in the online version of the journal.)

$A_2(-k\cos(\theta+iq))$ are introduced in the above integral to get

$$\Psi_e(x,y)=\frac{1}{\sqrt{2\pi}}\int_{-\infty}^{\infty}\left.\begin{matrix}A_1(-k\cos\theta)+qA_1'(-k\cos\theta)+\dfrac{q^2}{2!}A_1''(-k\cos\theta)+\cdots\\ A_2(-k\cos\theta)+qA_2'(-k\cos(\theta))+\dfrac{q^2}{2!}A_2''(-k\cos\theta)+\cdots\end{matrix}\right\}e^{ikR\cosh q}dq.$$

The second term in the above integral disappears during mathematical manipulations and consequently the integral then reduces to

$$\Psi_e(x,y)=\frac{1}{\sqrt{2\pi}}\int_{-\infty}^{\infty}\left.\begin{matrix}A_1(-k\cos\theta)+\dfrac{q^2}{2!}A_1''(-k\cos\theta)+\cdots\\ A_2(-k\cos\theta)+\dfrac{q^2}{2!}A_2''(-k\cos\theta)+\cdots\end{matrix}\right\}\times e^{ikR\cosh q}dq, \tag{51}$$

where $A_1(-k\cos\theta)$, $A_1''(-k\cos\theta)$, $A_2(-k\cos\theta)$ and $A_2''(-k\cos\theta)$ can be calculated from Equation (48). In fact, if $A_{1,2}(-k\cos(\theta_0+iq))$ may be extended in the neighborhood of $q=0$ (stationary point), then

$$\begin{cases}A_1(-k\cos(\theta+iq))=A_1(-k\cos\theta)+qA_1'(-k\cos\theta)+\dfrac{q^2}{2!}A_1''(-k\cos\theta)+O\left(q^3\right)\\ A_2(-k\cos(\theta+iq))=A_2(-k\cos\theta)+qA_2'(-k\cos(\theta))+\dfrac{q^2}{2!}A_2''(-k\cos\theta)+O\left(q^3\right)\end{cases}. \tag{52}$$

The intermediate range R_0 is supposed not to be at a far off distance. So one can apply a slightly modified version of the stationary phase method [23] to Equation (51). Thus, the diffracted field in the intermediate range is given as

$$\begin{aligned}\Psi_e(x,y)=&\frac{ik}{\sqrt{2\pi}}\left(\frac{\pi}{2kR}\right)^{1/2}\\&\times\left\{\begin{matrix}A_1(-k\cos\theta)\\A_2(-k\cos\theta)\end{matrix}\right\}\sin\theta\exp\left(ikR+i\frac{\pi}{4}\right)\\&+\left\{\begin{matrix}A_1''(-k\cos\theta)\\A_2''(-k\cos\theta)\end{matrix}\right\}\sqrt{\frac{2\pi}{(kR)^3}}\sin\theta\\&\times\exp\left(ikR+i\frac{\pi}{4}\right).\end{aligned} \tag{53}$$

where $A_1(-k\cos\theta)$, $A_2(-k\cos\theta)$, $A_1''(-k\cos\theta)$ and $A_2''(-k\cos\theta)$ can be calculated with the help of Equation (48). The expression given in Equation (53) gives the intermediate field asymptotic expression of the diffracted field while having asymptotic expansion of $\Psi_e(x,y)$ valid for any value of observation angle throughout the domain.

6. Numerical illustrations

In this section, the graphical behavior (energy radiated by the diffracted field) for different values of physical parameters such as incident angle, specific admittance parameter and wavenumber is discussed. We are interested to see how a finite barrier with impedance boundary conditions could be best used to reduce the sound intensity between a source and receiver. The scattering phenomenon is observed computationally by exhibiting the variation of amplitude of diffracted field [20 log] with the observation angle (Figures 1–4). Figures 1(*a*)–4(*a*) show the intermediate range solution for a plane wave incident at an angle $\theta_0=\pi/4$ on a conducting plate whereas Figures 1(*b*)–4(*b*) show the far-field solution for a plane wave incident. The diffracted field in the shadow region from the edge remains largely unchanged in both cases when $\theta_0=\pi/4$ and $\theta_0=-\pi/4$ due to the symmetry of the problem. In fact, the reciprocity theorem holds, that is, the ratio of pressure amplitude to source strength remains unchanged when we interchange the locations of the source and the receiver. It is concluded that the diffracted amplitude decreases considerably in the region $0<\theta<3\pi/4$ for intermediate range solution, whereas the amplitude increases when receiver is located in the same region (far-range). In each case, noise level is reduced considerably as the receiver approaches the finite conducting plate. A common observation can be made in all cases that there is an apparent reduction of sound intensity when source and receiver are taken in the intermediate range as compared to far-field results (by letting $R\to\infty$). The finite plate is assumed to be of length $2-$ units in each case.

In Figure 1(*a*) and (*b*), the results are presented for the case of intermediate and far-field approximations, respectively, for different values of incident angle θ_0 by fixing all other parameters. It is observed that the amplitude of the diffracted field in the intermediate zone is higher when position of line source is brought closer to the diffraction edge instead of lying far away. The fundamental trend for both the approximations appears to be different (one having a decreasing trend while the other is showing increasing trend up to certain values of observation angle θ). The amplitude for intermediate approximations has sharper peaks than for far-field approximations.

Figures 2(*a*)–3(*a*) and 2(*b*)–3(*b*) are plotted for different values of specific admittance when wavenumber is taken to be $k=1$ and $k=2$, respectively. Figures 2(*a*) and 3(*a*) are plotted for intermediate approximations while Figures 2(*b*) and 3(*b*) are plotted for far-field approximations. It can

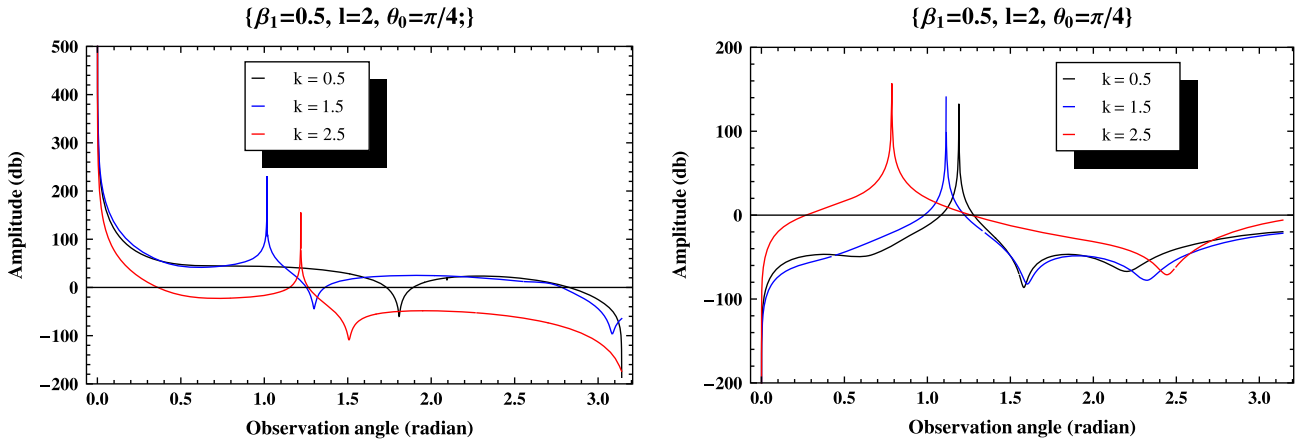

(*a*) Intermediate range solution (*b*) Far-field solution

Figure 4. Amplitude of the diffracted field vs. the observation angle for different values of wavenumber k when $l = 2$, $\beta_1 = 0.5$ and $\theta_0 = \frac{\pi}{4}$. (The colour version of this figure is included in the online version of the journal.)

be seen that the amplitude of the diffracted field increases by increasing the value of β_1 and causes little oscillation on increasing the value of k. In Figure 3(*a*), the region $5\pi/6 < \theta < \pi$ is showing a singular effect when the value of wavenumber is slightly increased up to one unit.

Figure 4(*a*) and (*b*) is plotted for intermediate and far-field approximations, respectively, by considering different values of wave number k. Here, the behavior of diffracted field does not deviate very much for different values of wave number k but overall the amplitude of the diffracted field is considerably larger as compared to other parameters θ_0, β_1 and the plate length l. It is mentioned that in Figures 2–4, the trends for both the intermediate approximations and far-field approximations are almost similar as observed in Figure 1(*a*) and (*b*).

7. Concluding remarks

An intermediate range solution for a plane wave incident on a finite conducting plate with different impedance boundary conditions on upper and lower faces is examined. Wiener–Hopf procedure is used to find an ultimate solution which is rigorous and uniformly valid (without restriction on the absorbing properties). The main idea behind the consideration of intermediate zone solution is to visualize the diffracted pattern more clearly than in far-field zone. It can be seen that the far-field solution and the intermediate zone solution differ by a multiplicative factor. In case of far-field approximation, the source position is assumed to be at a very large distance so that terms up to $O(1/\sqrt{kR})$ are retained while other terms are ignored where k is the R is the source to receiver distance. But, in the intermediate range solution, terms of $O(1/\sqrt[3]{kR})$ are also retained, that is, the position of source brought closer to the finite conducting plate. The term comprising $O(1/\sqrt[3]{kR})$ gives rise to an extra term in the diffracted field which produces a stronger field with more visible and clear diffraction pattern. The diffracted field for both, the far- and the intermediate-field approximations differ by a factor

$$\left\{ \begin{matrix} A_1''(-k\cos\theta) \\ A_2''(-k\cos\theta) \end{matrix} \right\} \sqrt{\frac{2\pi}{(kR)^3}} \sin\theta \exp\left(ikR + i\frac{\pi}{4}\right).$$

When $R \to \infty$, terms of $O(1/\sqrt[3]{kR})$ become negligible thereby rendering the solution valid over far-field range. Influence of various parameters on the diffracted field obtained via intermediate/far range approximation are presented and debated. Finally, it is substantiated that the intermediate range solution is a better choice as far as the accuracy of asymptotic expansion is concerned.

References

[1] Lighthill, M.J. *Proc. R. Soc. London* **1952,** *211,* 564–587.
[2] Curle, N. *Proc. R. Soc. London* **1955,** *231,* 505–514.
[3] Morse, P.M.; Ingard, K.U. *Acoustics I. Encyclopedia of Physics*; Springer: Berlin, 1961.
[4] Myers, M.K. *J. Sound Vib.* **1980,** *71,* 429–434.
[5] Rawlins, A.D. *Proc. R. Soc. Edinburgh: Ser. A* **1975,** *72,* 337–357.
[6] Asghar, S.; Hayat, T. *Acoust. Lett.* **1998,** *21,* 212–220.
[7] Ayub, M.; Naeem, A.; Nawaz, R. *Can. J. Phys.* **2009,** *87,* 1139–1149.
[8] Ayub, M.; Naeem, A.; Nawaz, R. *Comput. Math. Appl.* **2010,** *60,* 3123–3129.
[9] Ayub, M.; Ramzan, M.; Mann, A.B. *IEEE Trans. Antennas Propag.* **2009,** *57,* 1289–1293.
[10] Ayub, M.; Ramzan, M.; Mann, A.B. *J. Mod. Opt.* **2009,** *56,* 893–902.
[11] Nawaz, R.; Lawrie, J.B. *J. Acoust. Soc. Am.* **2013,** *134,* 1939–1949.
[12] Hoppe, D.J.; Rahmat-Samii, Y. *Impedance Boundary Conditions in Electromagnetics*; Taylor and Francis: Washington, DC, 1995.
[13] Senior, T.B.A.; Volakis, J.L. *IEEE Trans. Antennas Propag.* **1997,** *45,* 107–114.
[14] Nawaz, R. *Indian J. Pure Appl. Math.* **2012,** *43,* 571–589.

[15] Keller, J.B. *J. Opt. Soc. Am.* **1962,** *5,* 116–130.
[16] Imran, A.; Naqvi, Q.A.; Hongo, K. *Prog. Electromagn. Res.* **2007,** *75,* 303–318.
[17] Imran, A.; Naqvi, Q.A.; Hongo, K. *Opt. Commun.* **2009,** *282,* 443–450.
[18] Chakrabarti, A. *Indian J. Pure Appl. Math.* **1977,** *8,* 702–717.
[19] Lawrie, J.B.; Abrahams, I.D. *J. Eng. Math.* **2007,** *59,* 351–358.
[20] Senior, T.B.A.; Volakis, J.L. *Approximate Boundary Conditions in Electromagnetics*; The Institution of Electrical Engineers: London, 1995.
[21] Pelosi, P.; Ufimtsev, P.Y. *IEEE Trans. Antennas Propag., Magazine*, **1996,** *38,* 31–35.
[22] Noble, B. *Methods Based on the Wiener-Hopf Technique*; Pergamon: London, 1958.
[23] Copson, E.T. *Asymptotic Expansions*; Cambridge University Press: New York, 1967.
[24] Asghar, S.; Hayat, T.; Asghar, B. *Mod. Opt.* **1998,** *3,* 515–528.
[25] Jones, D.S. *Q. J. Math.* **1952,** *3,* 189–196.
[26] Ayub, M.; Nawaz, R.; Naeem, A. *J. Math. Anal. Appl.* **2009,** *349,* 245–258.